Investigation and Numerical Analysis of Strain Distribution in the Twist Extrusion of Pure Aluminum

Seyed Ali Asghar Akbari Mousavi and Shahab Ranjbar Bahador

The effects of performing three twist extrusion passes on high purity aluminum samples were studied in this paper in regard to numerical analysis and experimental studies. The finite element analysis of the von-Mises stress and the equivalent plastic strain in the outer longitudinal and transverse cross-sections, which are parallel and normal to the billet axis respectively, was carried out. The simulation results showed that the end of the workpiece underwent more equivalent plastic strains in contrast to the head of the sample. Moreover, the corner regions experienced more strains than the center zone did. However, the heterogeneity in strain distribution in both longitudinal and transverse cross-sections decreased by performing the sequential twist extrusion passes. The experimental outcomes such as microstructure evolutions, microhardness and tensile tests validated the simulation results.

INTRODUCTION

Recently, employing the polycrystalline materials through the severe plastic deformation (SPD) methods has been the essence of metal forming research to produce ultra-fine and nano-grain structures.[1] SPD includes several different techniques such as equal channel angular pressing (ECAP),[2] high pressure torsion (HPT),[3] accumulative roll bonding (ARB),[4] multi-directional forging (MDF),[5] repetitive corrugation and strengthening (RCS),[6] and a rather newly developed method called twist extrusion (TE)[7–9] introduced by Beygelzimer et al.[10] in 1999. A workpiece is extruded by hydrostatic pressure through a twisted channel with a rotation angle (α) and a slope angle (β). Figure 1 shows a schematic representation of the workpiece during the TE process. The billet transverse cross-section is normal to the extrusion direction, and it remains constant after the process.

Since the microstructure and the mechanical properties of the deformed material depend upon the strain distribution, this study has been conducted to understand the mechanism of strain-induced deformation during the three passes of TE process. The manner in which strain distribution occurs across the material during the twist extrusion process determines the grain size distribution. Therefore, knowing the mechanism of strain distribution all over the sample may help to produce a microstructure with finer grains and to achieve a workpiece with homogenous mechanical properties.

Earlier studies simulated the strains difference across the transverse cross-section of a Ti-6Al-4V billet.[11] Begelzimer et al.[12] modeled the strain distribution and the velocity field on the billet transverse cross-section. Orlov et al.[13,14] analyzed the microstructure evolutions of Al 1100 by TEM and examined the macro-flow patterns and mechanical properties of this material as a continuation of the earlier investigations.[15] In this study, the finite element analysis of the von-Mises stress and the equivalent plastic strain (PEEQ) along the outer longitudinal and transverse cross-sections (***A*** and ***D***) of a commercially pure aluminum billet during three TE passes is presented. Simulation outcomes were verified by experimental results.

How would you…

…describe the overall significance of this paper?

The effects of performing three twist extrusion passes on high purity aluminum samples were studied in regard to numerical analysis and experimental studies. The simulation results showed that the end of the workpiece underwent more equivalent plastic strains in contrast to the head of the sample. Moreover, the corner regions experienced more strains than the center zone did. The experimental outcomes such as microstructure evolutions, microhardness and tensile tests validated the simulation result.

…describe this work to a materials science and engineering professional with no experience in your technical specialty?

The twist extrusion process can produce ultafine grains without changing the sample's cross section. The mechanical strength and hardness of the samples are increased by performing three twist extrusion passes. The heterogeneity in strain distribution in both longitudinal and transverse cross section decrease by performing the sequential twist extrusion passes.

…describe this work to a layperson?

In the twist extrusion process, a workpiece is extruded by hydrostatic pressure through a twisted channel with a predetermined rotation and twisted angles. Since the microstructure and the mechanical properties of the deformed material depend upon the strain distributions, this study was conducted to understand the mechanism of strain induced deformation during the three passes of the twist extrusion passes. Knowing the mechanism of the strain distributions all over the sample would help to produce a microstructure with finer grains and to achieve a workpiece with homogenous mechanical properties.

FEM DETAILS

The finite element analysis of the TE process was carried out by using the elasto-plastic finite element (FEM) code, ABAQUS 6.5.[16] The initial dimensions of workpiece were 70×32×18

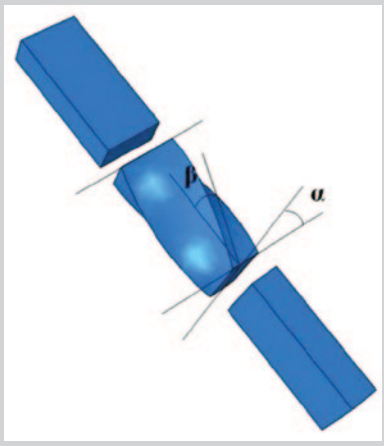

Figure 1. Schematic of the workpiece during the twist extrusion process.

Equations

$$\bar{\sigma} = [A + B(\bar{\varepsilon}^{pl})^n]\left[1 + C\ln\left(\frac{\dot{\bar{\varepsilon}}^{pl}}{\dot{\varepsilon}_o}\right)\right]\left(1 - \hat{\theta}^m\right) \quad (1)$$

$$\hat{\theta} \equiv \begin{Bmatrix} 0 \\ 1 \end{Bmatrix} \begin{matrix} \text{for } \theta < \theta_{transition} \\ \theta - \theta_{transition} / \theta_{melt} - \theta_{transition} \text{ for } \theta_{transition} \le \theta \le \theta_{melt} \\ \text{for } \theta > \theta_{melt} \end{matrix} \quad (2)$$

$$\tau = mk \quad (3)$$

mm^3. The isometric view of the partial discretized model is shown in Figure 2. This figure also illustrates the positions of the element numbers of 4, 24, 44, 64, and 244. These elements were chosen since they experience different strains.[11,17] Four guides and three dies were used to adjust the setup for three accumulated passes as shown in Figure 3. The lengths of the four guides were 60 mm, 20 mm, 20 mm and 60 mm respectively. The dies had the dimensions of 25 mm radius and 25 mm thickness, including a twisted channel with a rectangular cross-section of 18×32 mm^2 and the clockwise rotation angle (α) of 60° and the slope angle (β) of 90°. The ram speed was 3 mm/s and the friction coefficient between the die and the sample surfaces was 0.01. The dies, the ram and the guides were modeled as rigid solid type, and therefore they were assigned no material property. The dynamic temperature-displacement explicit procedure was used for the finite element analysis.

The Johnson–Cook material model[16,18] was used (Equation 1) to describe the behavior of the material during the deformation. The Johnson–Cook constitutive equation is defined as: Equation 1, where $\bar{\sigma}$ is the yield stress at non-zero strain rate, $\bar{\varepsilon}^{pl}$ is the equivalent plastic strain, $\dot{\bar{\varepsilon}}^{pl}$ is the equivalent plastic strain rate for $\dot{\varepsilon}_0$ = 1.0 s^{-1}. ***A***, ***B***, ***C***, ***n*** and ***m*** are the material parameters measured at or below the transition temperature, $\theta_{transition}$. The material constants were determined from straining tests performed in tension. The mechanical properties of the materials, used in this study, and their Johnson–Cook parameters are given in Table I.[19] $\hat{\theta}$ is the nondimensional temperature defined as Equation 2, where θ is the current temperature, θ_{ratio} is the melting temperature, and $\theta_{transition}$ is the transition temperature defined as the one at or below which there is no temperature dependence on the expression of the yield stress.

The expression in the first set of the brackets gives the stress as a function of strain for $\bar{\varepsilon}^{pl}$ = 1.0 and $\hat{\theta}$ = 0. The expressions in the second and the third brackets represent the effects of strain rate and temperature respectively. At the melting temperature ($\hat{\theta}$ = 1), the stress approaches zero for all strains and strain rates.

The frictional shear stress ***τ*** for all of the contact surfaces was defined as Equation 3, where ***m*** is the friction factor and ***k*** is the shear flow of the material. A friction factor of m = 0.01 was considered for all contact surfaces.

Dynamic temperature-displacement type of the explicit method was used to express large deformations. The billet and the die contact were modeled with surface to surface finite sliding contact pair algorithm. The frictional form of this algorithm was also used to model the ram contact with the billet. The separable contact algorithm was used for describing the die and the billet contact

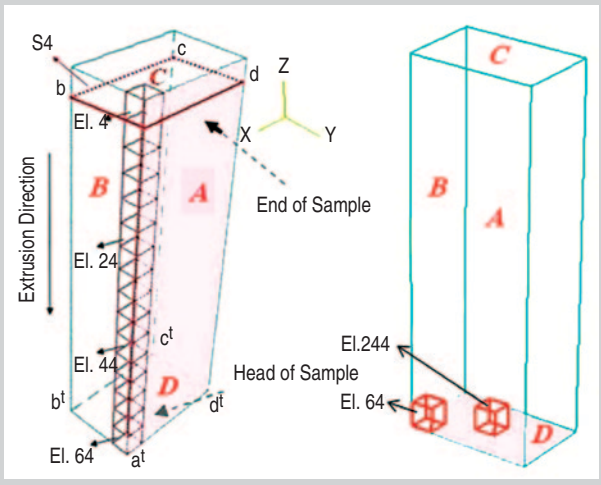

Figure 2. Partial discretized sample models with element numbers of 4, 24, 44, and 64 in plane ***A*** and element numbers of 64 and 244 in plane ***D***.

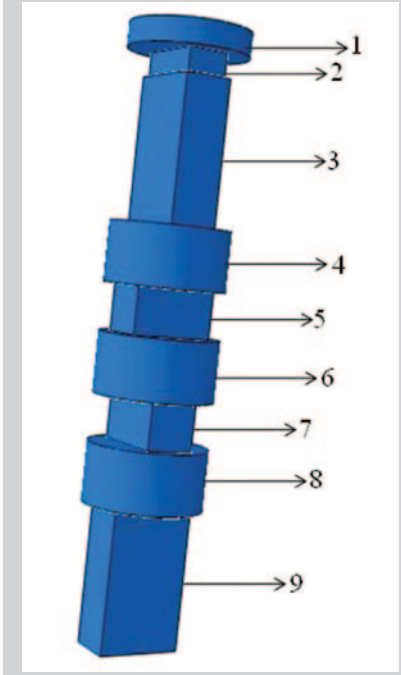

Figure 3. Schematic of TE setup for three passes: (1) ram, (2) billet, (3) the first guide, (4) the first die, (5) the second guide, (6) the second die, (7) the third guide, (8) the third die, and (9) the fourth guide.

EXPERIMENTAL STUDIES

A billet of commercial purity aluminum (99.7%) with primary dimensions of 70 × 32 × 18 mm^3 was used as the material for the investigation. The chemical composition of the pure aluminum is 99.7Al-0.13Fe-0.07Si-0.04Cu-0.02Zn-0.02Pb-0.008V-0.005Mg-bal. other. The billet was annealed at 773 K for 2.5 hours and then air quenched. Afterwards, it passed through the twisted channel of the TE die with the slope angle (β) of 60° and the rotation angle (α) of 90°. TE was performed for three passes at room temperature.

The microstructures of the TEed samples were examined by optical microscopy of Olympus, making a comparison between different regions according to the elements positions in simulation process (see Figure 2). The tensile tests were carried out using a Santam STM-20 testing machine with the maximum load of 10 KN at room temperature and the strain rate of 3×10^{-3} s^{-1}. The dog-bone flat specimens with the dimensions of 5 × 3 × 2 mm^3 were cut in the longitudinal direction of the billet in accordance with elements positions (see Figure 2).

The hardness tests were performed on the samples prepared for microstructure observations by ESEWAY hardness tester. The Vickers microhardness tests (Hv) were employed by using 30 g loads for the samples before and after TE process. At least five separate measurements were performed on each sample.

surfaces. The non-separable contact algorithm was used for describing the ram and the billet contact surfaces.

Boundary conditions were chosen to be like the practical case. Therefore, the six freedom degrees of the dies were foreclosed, and the ram could move only in the direction parallel to the billet axis during the deformation. In addition, the initial temperature of the billet was set to 298 K as the thermal boundary condition. The 8-nodes thermally coupled brick elements with tri-linear displacement were used. Also the 2 mm billet mesh size was used.

RESULTS

von-Mises Stress Distribution

Figure 4 shows the von-Mises stress contours of the sample during 20 steps of the deformation. The ram and the other assembly features have been removed for better clarification. It is obvious that the maximum stress occurs in corners, because these regions are in contact with the die interior surfaces. Figure 5 illustrates the von-Mises stress contours of four different stages with color map, selected from the stages of (5), (10), (15), and (20) in Figure 4, respectively. Figure 5a shows the deformed billet during the first TE pass, where the maximum stress is about 259 MPa. As it is illustrated in Figure 5b and c the maximum stress during the second and the third passes of TE are about 364 MPa and 445 MPa, respectively. It means that the stress increase is not the same in three passes, and the stress intensity decreases by performing further passes. The variations of von-Mises stress versus time are illustrated in Figure 6. Each curve is divided into seven parts. Three of them refer to the different TE passes and the other parts relate to the time in which billet passes through the guides. All of these regions are defined in Figure 6 for two elements of 64 and 4. The separate regions for the elements of 24, 44, and 244 are similar to the elements of 64 and 4, respectively, which were described in Table II. The amounts of stresses during all the stages and their related time steps are summarized in Table II. Though during the first pass of TE the billet experiences the maximum stress values along the ***aa′***, but the amounts of performed stress are not the same along this line. The end

Table I. Johnson–Cook Model Parameters for Pure Aluminum[20]

A (MPa)	B (MPa)	n	C	m	T_m (K)
80	120	0.73	0.008	1.7	933

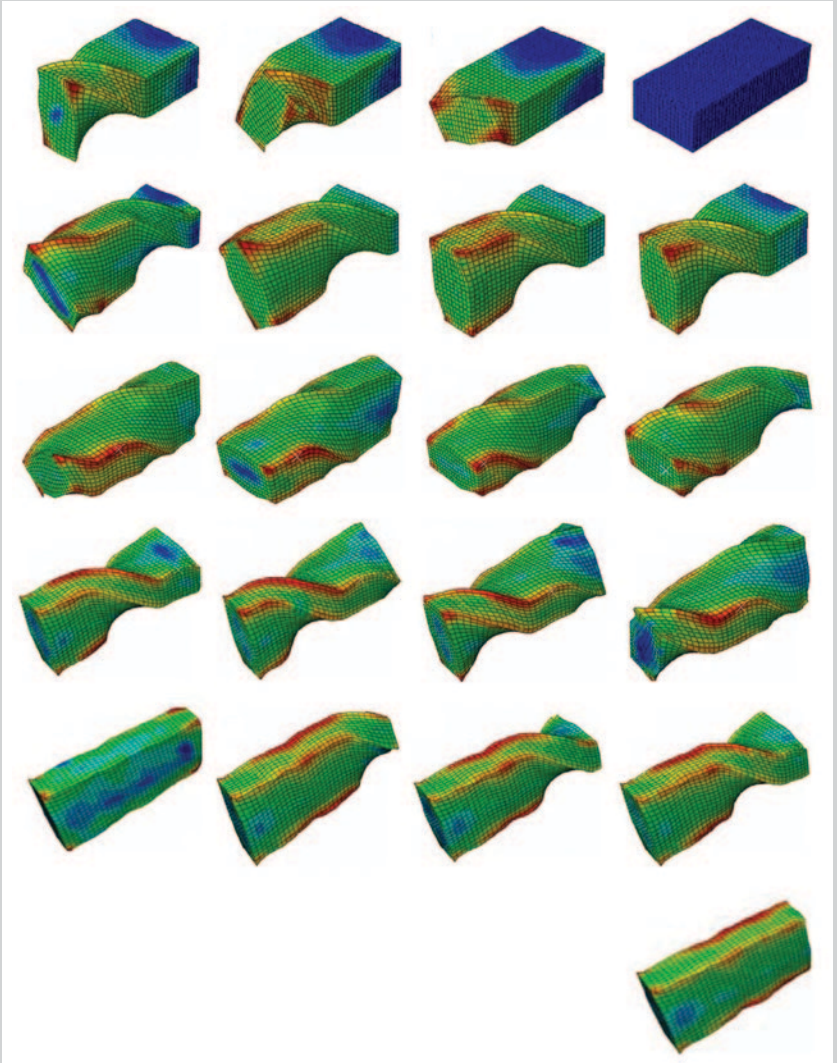

Figure 4. The von-Mises stress contours of pure aluminum sample during 20 steps of the deformation, arranged from right to left.

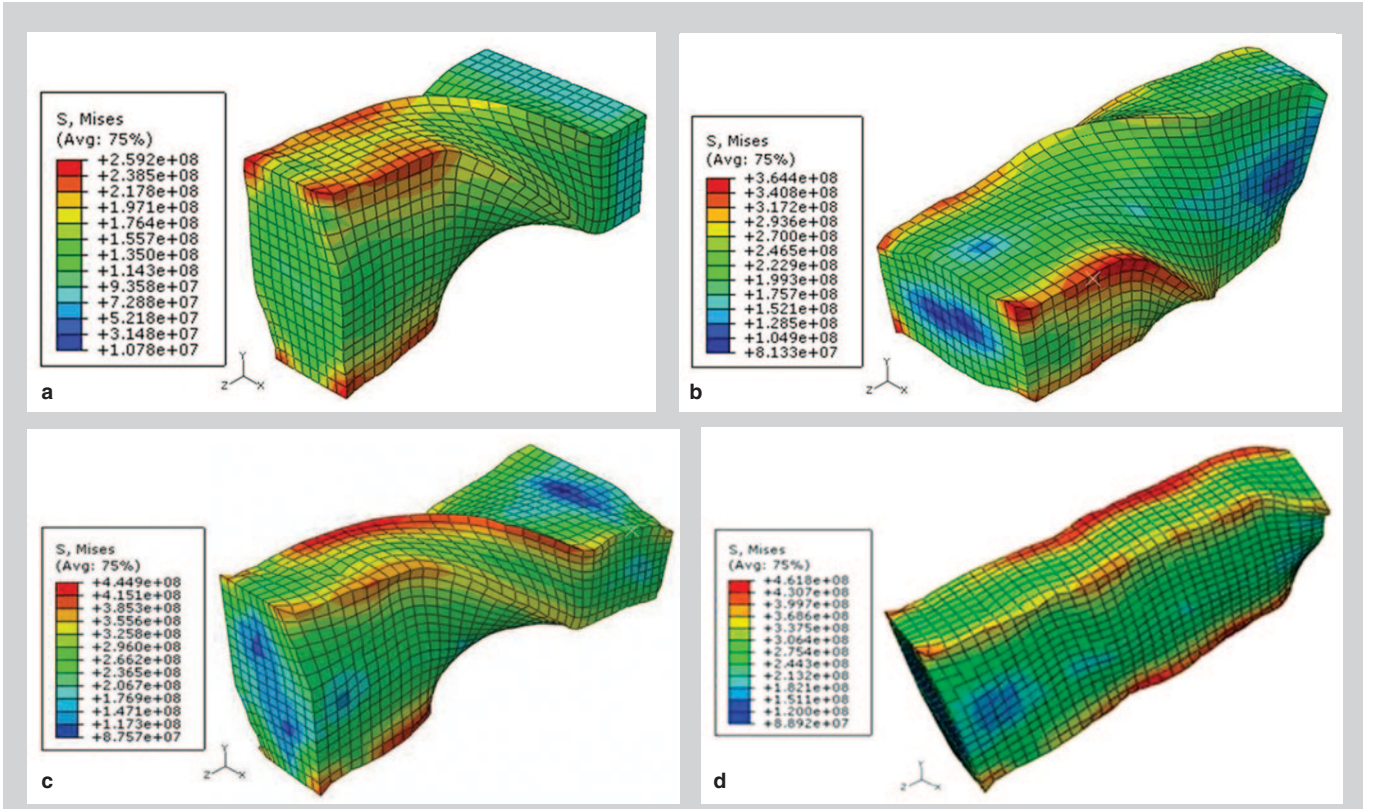

Figure 5. Four von-Mises stress contours selected from Figure 4 in (a) the 5th, (b) the 10th, (c) the 15th, and (d) the 20th steps.

of the sample undergoes the stress of 305 MPa, while the head of the sample experiences the von-Mises stresses of 185 MPa and 150 MPa, in corner and center, respectively. The resultant stresses during the next TE passes are considerably less than the first pass, as the stress magnitudes during the third TE pass for element numbers of 244, 64, and 4 are 45 MPa, 85 MPa, and 40 MPa, respectively.

Equivalent Plastic Strain Distribution

Figure 7 illustrates the PEEQ contours of four different stages with color map, selected from the 5th, 10th, 15th, and 20th stages of three TE process. As it can be predicted by stress contours, the edge ***aa′*** undergoes the most strains. Figure 8 illustrates the diagram of the PEEQ versus time for the element numbers of 4, 24, 44, 64, and 244 during three TE passes. As shown in Figure 8, after the first pass, the element number of 4 reaches the maximum strain of 2.30, and by moving along the billet axis from the upper surface toward the lower surface (the end to the head) of the workpiece, the PEEQ decreases. Moreover, the decrease of PEEQ occurs by moving from corner to the center in section ***D*** of the sample. The magnitudes of PEEQ for elements 24, 44, 64, and 244 are 1.30, 1.20, 0.85, and 0.45, respectively. However, as shown in Table III, the billet undergoes more strains in the first two TE passes than in the third pass, which is in accordance to the stress variations summarized in Table II.

Microstructure Evolution

Figure 9a shows the microstructure of as-annealed sample having the average grain size of 859 μm. Figure 9b–g illustrates the microstructures of the corner and the center regions in plane ***A*** and ***D*** according to the Figure 2. As it is indicated in Figure 9b–d the mean grain size decreases substantially throughout the both cross-sections by employing the first pass of TE. However, the decrease of grain size varies in different positions, as the mean grain size in elements 4, 64, and 244 are 103 μm, 132 μm, and 155 μm, respectively. Nevertheless, initial grains are observable in the deformed structure, meaning that the performed strain during the first pass of TE does not affect the microstructure completely. Careful inspection in Figure

Table II. The Values of von-Mises Stresses, Equivalent Plastic Strains (PEEQ), and the Time Steps for Three Passes of TE

Element Number	4	24	22	62	244
Time Step(s)					
1st Pass	10–40	10–40	0–20	0–20	0–20
2n Pass	45–60	45–60	25–45	25–45	25–45
3rd Pass	65–80	65–80	50–75	50–75	50–75
Von-Mises Stress (MPa)					
1st Pass	305	225	218	185	150
2nd Pass	50	80	85	60	60
3rd Pass	40	70	79	85	45
Equivalent Plastic Strains (PEEQ)					
1st Pass	2.30	1.30	1.20	0.85	0.45
2nd Pass	1.15	1.10	1.10	0.75	0.40
3rd pass	0.75	1.10	1.00	0.70	03.0

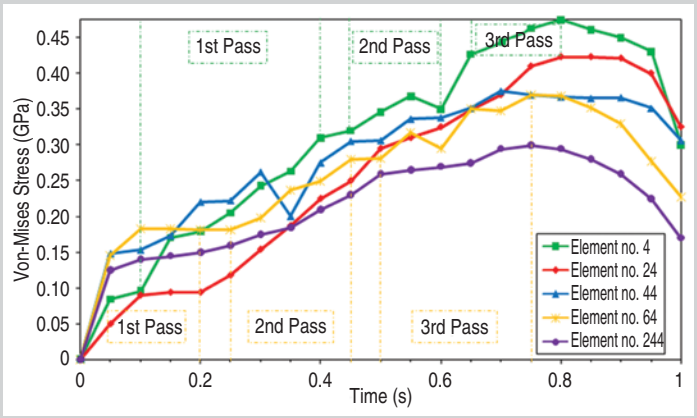

Figure 6. The variations of von-Mises stress versus time during three TE passes for the element numbers of 4, 24, 44, 64, and 244.

9e–g illustrates that performing the third TE pass produces finer grains of 30 µm, 43 µm, and 55 µm for the element numbers of 4, 64, and 244, respectively.

Mechanical Properties

The average Vickers microhardness of the annealed workpiece is about 23 Hv. Figure 10a shows that after performing the first pass of TE, the Vickers microhardness reaches the maximum of 38.18 Hv in ***a***. However, the hardness distribution is not homogeneous across the plane ***A***, and one edge has slightly more hardness in contrast to the opposite side. That is, two neighboring corners of ***a*** and ***b*** situated in the plane ***A*** have different mechanical properties. Figure 10a illustrates that in the upper region encompassing element number of 4, the corner ***a*** has the hardness value of 38.18 Hv, while the opposite corner of ***b*** has the hardness of 34.40 Hv. A similar trend occurs all over the plane ***A***. On the other hand, the Vickers microhardness values decrease at edge ***aa′*** from the end to the head of the sample (38.18 Hv to 30.40 Hv).

Employing the second TE pass improves the Vickers microhardness value throughout the plane ***A*** with a range from 34.40 Hv to 42.58 Hv as indicated in Figure 10b. Similarly, carrying on the third TE pass increases the hardness of the head and the end of the sample to the values of 39.66 Hv and 45.57 Hv, respectively (see Figure 10c).

The microhardness variation has different pattern throughout the plane ***D***. Performing the first TE pass enhances the microhardness in transverse cross-section heterogeneously, as the most microhardness value of 34.4 Hv is created in corners, and it decreases to 27 Hv by moving toward the center. The next TE passes have the same trend, causing the microhardness increase in the corners to 37.30 Hv and 40.70 Hv and in the center to 31.70 Hv and 36.60 Hv, respectively.

Table III summarizes the results of the tensile test conducted in positions according to Figure 2. Employing the first pass of TE increases the ultimate tensile strength by about 2 times. It also enhances the yield strength nearly 3 times. However, the head and the end of the sample have different strength properties. Table III shows that the tensile and the yield strengths increase from the head of the sample (element no. 64) toward the end of the sample (element no. 4). Also, the strength properties enhance by moving from center towards corner in plane ***D***. This plane has less strength properties in contrast to the plane ***A***. Table III shows though the third pass of TE increases the yield and the tensile strength, it has less enhancing effects

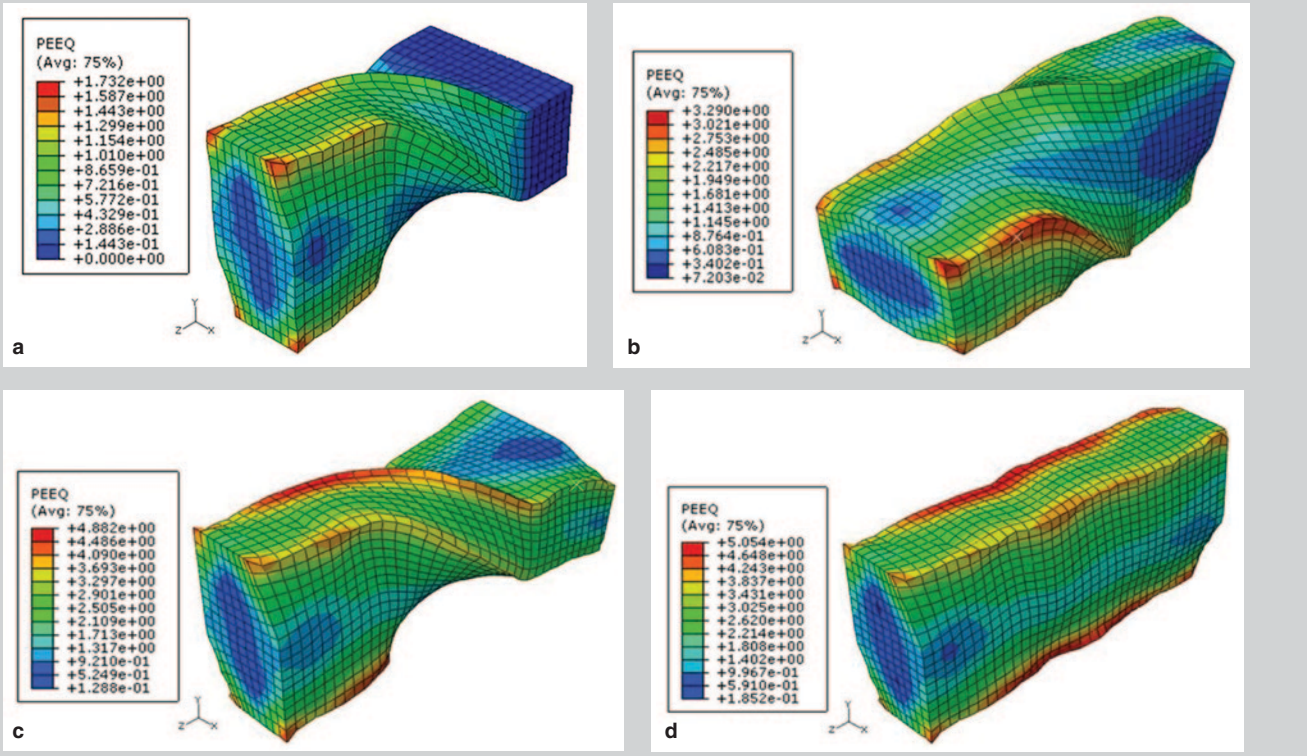

Figure 7. Four equivalent plastic strain (PEEQ) contours with color map, related to (a) the 5th, (b) the 10th, (c) the 15th, and (d) the 20th steps.

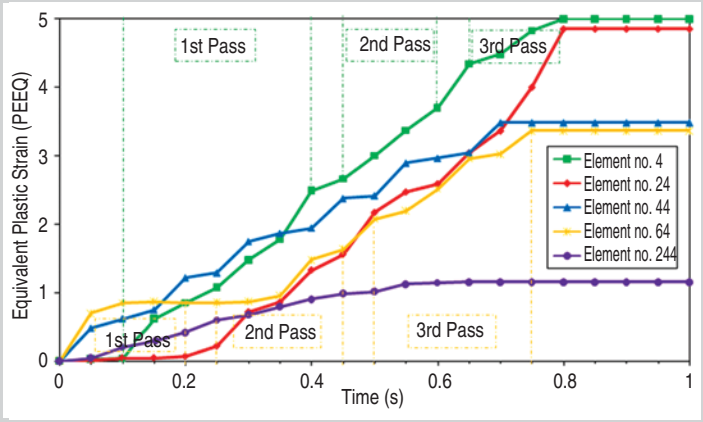

Figure 8. The variations of equivalent plastic strain (PEEQ) versus time during three TE passes for the element numbers of 4, 24, 44, 64, and 244.

than the first and the second TE passes.

On the other hand, the ductility properties including the uniform elongation and the elongation to failure decrease by performing TE passes. This decrease is different throughout the model. In plane ***D*** the center zone has better ductility properties than the corners, and in plane ***A*** the end of the sample has weaker ductility in contrast to the head of the sample. This dissimilarity decreases by performing the sequential TE passes.

DISCUSSION

It is important to recognize that the present analysis provides some information on the microstructure and mechanical heterogeneity along the longitudinal and transverse cross sections (***A*** and ***D***) which are parallel and normal to the billet axis, respectively.

The examination of von-Mises stress in plane ***D*** shows that the stresses are more intensive in peripheral regions (element no. 64) than center parts (element no. 244), which is probably due to the friction between the die interior surfaces and sample exterior surfaces (see Figure 5). This heterogeneity decreases by performing the next passes, because the internal stresses which are more intensive in peripheral regions oppose the new external stresses produced during external TE passes, and as a result, the von-Mises stresses in these regions decreases. The condition in center zone is vice versa. The internal stress remaining from the first TE pass is weaker than at the corners, causing less decrease in the new external stresses during the next TE passes. As a consequence of these two reactions the distribution of von-Mises stress becomes more homogeneous throughout the plane ***D***.

On the other hand, an observable stress discrepancy can be seen along the edge ***aa′*** in plane ***A***. As Figure 6 illustrates the end of the workpiece experiences the most stress in contrast to the head of the sample. As a comparison between two elements of 64 and 4 after the first TE pass, the von-Mises stresses in these regions are 185 MPa and 305 MPa, respectively (see Table II). While the billet passes through the die, the residual stresses in lower parts act as the backpressure, heightening the performed stresses in the end of the sample, and as a result, it increases the von-Mises stresses in the end regions in contrast to the head zone.

During the second and the third TE passes the stresses lessen significantly all over the plane ***A***. Though the element of 4 has the most stress in the first pass, it undergoes the least stress after the third pass. This indicates that the stresses in the head regions decrease during the second and the third TE passes, weakening the backpressure which has a noticeable role in the von-Mises stresses.

The PEEQ contours in Figure 7 are in accord with the von-Mises stresses distribution. In plane ***D*** the element number of 244 undergoes less strain than the element number of 64. In plane ***A*** the head of the sample has the minimum strain, and by moving toward the end of the sample the strain value enhances, as the maximum value of strain occurs in the end of the workpiece. The reason might be the different mode of the deformation during the TE process. The mode of the deformation in the head of the sample is simple shear in the transverse section, which does not substantially affect section ***A***.[17] The deformation mode in the central region is divided into two distinctive modes: the inner part where the mode of deformation is simple shear in plane ***A***, encompassing the PEEQ of $0.2 < e < 0.4$, and the peripheral region where the mode of deformation is severe simple shear in

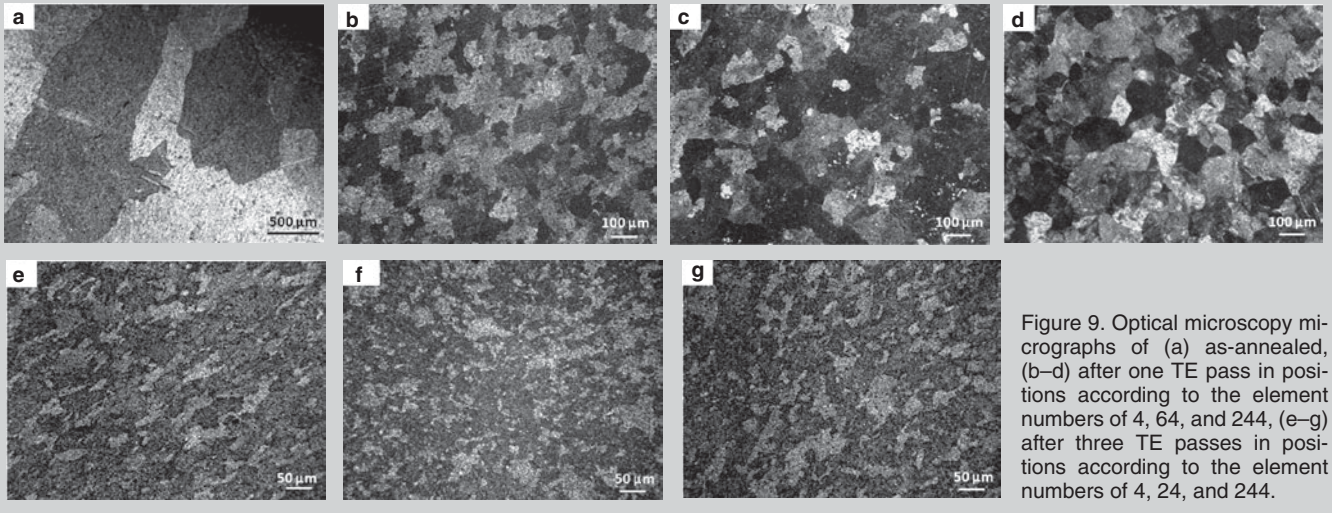

Figure 9. Optical microscopy micrographs of (a) as-annealed, (b–d) after one TE pass in positions according to the element numbers of 4, 64, and 244, (e–g) after three TE passes in positions according to the element numbers of 4, 24, and 244.

plane ***A***, and it experiences an equivalent strain of e ~ 2.[17] Because of the symmetrical geometry of the sample, it was believed that the ends of the sample have strain values similar to the head of the sample. However, this study shows that the strain magnitudes are more in the end of the sample than in the head of the sample due to the enlarging stress (Figure 8 and Table II).

As the von-Mises stress intensity decreases by increasing the pass numbers, the strain magnitude also decreases all over the workpiece. However, this decrease is not comparable in different regions, and has the pattern of von-Mises stress.

Figure 9b and c shows the microstructures of the end and the head of the billet along the ***aa′*** after one TE pass. The grain size is reduced in both regions, as this reduction is more observable in the end of the sample than in the head of the sample. However, the initial grains are distinguishable in both areas, which is in accordance with the earlier works.[15] Figure 9d illustrates the microstructure of the center zone in plane ***D***, which includes larger deformed grains and also more initial grains in comparison with the microstructures of plane ***A*** (Figure 9a and b). This is in accordance with the PEEQ distribution. With the third TE pass, the average grain size in all mentioned positions decreases noticeably (Figure 9e–g). Furthermore, the grain size difference throughout both planes ***A*** and ***D*** decreases significantly, and the grains are formed according to the vortex-like flow of TE.[15,17] As a comparison, the resultant mean grain size from this process is comparable with the ECAP process. As a case in point, Skortzki et al.[20] carried out three ECAP passes using route A on pure aluminum, which decreased the mean grain size from 280 μm in initial state to about 62 μm after three ECAP passes in outer longitudinal plane while performing three TE passes decreased the initial mean grain size of 859 μm to 43 μm.

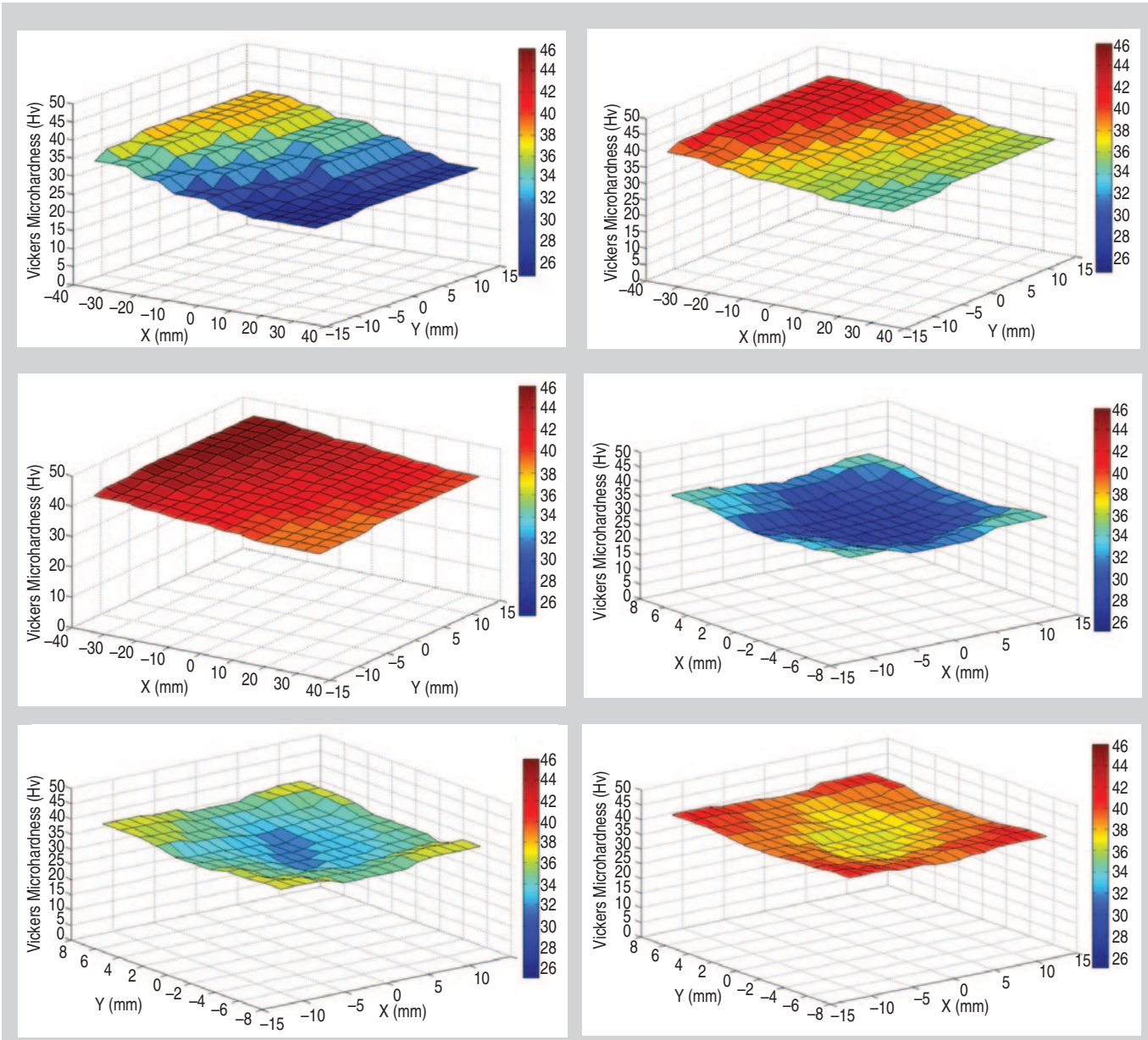

Figure 10. The hardness profiles of the plane ***A*** for a pure aluminum billet after (a) one TE pass, (b) two TE passes and (c) three TE passes and the hardness profiles of the plane ***D*** (d) one TE pass, (e) two TE passes and (f) three TE passes.

Table III. The Strength and the Ductility Properties of Pure Aluminum during Three Passes of TE in Positions According to the Element Numbers of 4, 24, 44, 64, and 244

Specimen Condition	Element Number	Yield Strength (MPa)	Tensile Strength (MPa)	Uniform Elongation (%)	Uniform Elongation (%)
As-annealed	4	31.30	57.34	16.32	42.36
	24	33.53	61.13	18.95	47.65
	44	32.46	60.20	19.27	49.15
	64	31.81	59.48	16.31	45.33
	244	32.13	61.52	17.84	42.77
1 TE Pass	4	93.12	128.20	8.34	29.83
	24	88.24	122.84	8.92	31.56
	44	84.61	113.57	11.32	33.76
	64	82.15	96.36	10.39	33.26
	244	65.48	82.97	12.46	35.20
2 TE Passes	4	153.20	161.37	4.68	22.19
	24	146.85	155.46	5.31	23.78
	44	145.67	153.13	6.71	23.12
	64	130.45	142.15	6.45	26.54
	244	121.45	130.73	6.81	26.15
3 TE Passes	4	172.48	184.38	3.55	22.41
	24	165.24	178.55	3.29	23.67
	44	157.51	177.33	4.11	22.41
	64	155.62	171.20	4.57	25.50
	244	149.40	163.73	4.84	24.30

Figure 10a–c illustrates the three-dimensional microhardness profiles throughout the plane ***A*** during the three passes of TE. As can be seen after the first TE pass by moving from the head to the end of the sample, the hardness magnitudes increase. However, the hardness distribution across the plane ***A*** is not homogenous (Figure 10a). That is, the magnitude of hardness is higher in edge ***aa′***, which lessens by moving toward the edge ***bb′*** This phenomenon might be due to the route of the TE processing that employing sequential clockwise routes gives rise to producing different microstructures and mechanical properties at each neighboring corner in plane ***A***.[17] It can be concluded from Figure 10b and c that conducting next TE passes decreases the hardness distribution heterogeneity. The difference of hardness values between the upper and the lower surfaces of the workpiece during three different passes of TE is 11.38 HB, 9.18 HB, and 5.91 HB, respectively. This means that repeated passes of TE homogenize the microhardness distribution along the plane ***A***.

However, microhardness distribution in plane ***D*** differs from plane ***A***. Figure 10d shows that by performing the first TE pass the microhardness increases in the corners more than in the center. Figure 10e and f illustrates that the sequential TE passes moderate this hardness difference in plane ***D***, as the microhardness differences during three TE passes is 7.4, 5.6, and 4.1, respectively.

Similar trends also occurred in the strength properties summarized in Table III. By increasing the number of passes the strength difference between various elements reduces, which is in accordance with the microstructures and the hardness outcomes. Table III indicates that the third TE pass has less enhancing effects on strength properties. Therefore, by performing the next TE passes the strain increase in the head region is more than in the end zone. The strain enhances until both the lower and upper regions achieve the saturation limit, and as a result the strength properties become reasonably homogeneous. In a comparison between the head and the end of the billet in plane ***A*** (element numbers of 64 and 4) in regard to the tensile strength, the difference of strength values during the first, the second and the third TE passes is 31.48 MPa, 19.22 MPa, and 13.18 MPa, respectively. Similar comparison in plane ***D*** between the corner and the center regions (element numbers of 64 and 244) results in 13.39 MPa, 11.42 MPa, and 7.47 MPa values, respectively, during three TE passes. These outcomes show that the repeated passes of TE have a homogenizing effect throughout the sample. This might be attributed to the fact that the end of the sample reached the saturation limit earlier than the head of the sample and therefore more passes may reduce the strain heterogeneity throughout the sample.

Table III shows that the third TE pass enhances the average yield and the tensile strengths along the edge ***aa′*** from the initial state of 36 MPa and 60 MPa to 164 MPa and 178 MPa, respectively. The resultant yield and tensile strengths results are comparable with those achieved from three ECAP passes, in which the tensile strength of pure aluminum increased from 60 MPa to 158 MPa.[21]

References

1. R.Z. Valiev, R.K. Islamgaliev, and I.V. Alexandrov, *Prog. Mater. Sci.,* 45 (2000), pp. 103–189.
2. V.M. Segal, *Mater. Sci. Eng. A*, 197 (1995), pp. 157–164.
3. N.A. Smirnova et al., *Fiz. Met. Metalloved.*, 61 (1986), pp. 1170–1177.
4. Y. Saito et al., *Scr. Mater.,* 39 (1998), pp. 1221–1227.
5. G.A. Salishchev, O.R. Valiakhmetov, and R.M. Galeyev, *J. Mater. Sci.*, 28 (1993), pp. 2898–2903.
6. J.Y. Huang et al., *Acta Mater.*, 49 (2001), pp. 1479–1505.
7. R.Z. Valiev et al., *JOM*, 58 (4) (2006), pp. 33–39.
8. Y. Beygelzimer et al., *Solid State Phenom.*, 114 (2006), pp. 69–78.
9. Y.Y. Beygelzimer et al., *Phys. Technol. High Pressure*, 9 (1999), pp. 109–110.
10. Y. Beygelzimer, D. Orlov, and V. Varyukhin, *Ultrafine Grained Materials II*, ed. Y.T. Zhu et al. (Warrendale, PA: TMS, 2002), pp. 297–304.
11. S.A.A. Akbari Mousavi, A.R. Shahab, and M. Mastoori, *Mater. Des.*, 494 (2008), pp. 1316–1329.
12. Y. Beygelzimer et al., *J. Mater. Process. Technol.*, 209 (2009), pp. 3650–3656.
13. D. Orlov et al., *Mater. Trans.*, 49 (2008), pp. 2–6.
14. D. Orlov et al., *Mater. Trans.*, 50 (2009), pp. 96–100.
15. D. Orlov et al., *Mater. Sci. Eng. A*, 509 (2009), pp. 105–111.
16. Abaqus, Rel. 6.5 (Dassault Systèmes Simulia Corp., SIMULIA, Rising Sun Mills, 166 Valley Street, Providence, RI 02909-2499).
17. Y. Beygelzimer et al., *Mater. Sci. Eng. A*, 503 (2009), pp. 14–17.
18. G.R. Johnson and W.H. Cook, *Proceedings of the 7th International Symposium on Ballistics* (Arlington, VA: ADPA, 1983), pp. 541–547.
19. S.A.A. Akbari Mousavi and A.R. Shahab, *Int. J. Mod. Phys. B*, 22 (2008), pp. 2858–2865.
20. W. Skortzki et al., *Acta Mater.*, 55 (2007), pp. 2211–2218.
21. A. Sivaraman and U. Chakkingal, *J. Mater. Process. Technol.*, 202 (2008), pp. 543–548.

Seyed Ali Asghar Akbari Mousavi, associate professor, and Shahab Ranjbar Bahadori, research associate, are with the School of Metallurgy and Materials Engineering, University College of Engineering, University of Tehran, P.O. Box: 11155-4563, Tehran, Iran. Dr. Akbari-Mousavi can be reached at akbarimusavi@ut.ac.ir.